Draft to be published: Langmuir, 2020, 36 (8), 1864-1870.

Electrochemical Deposition of Polyelectrolytes is Maximum at the Potential of Zero Charge

David Moore, [†,§] *Jennifer A. Arcila,* [†,§] *Ravi F. Saraf* [*†‡]

†Department of Chemical and Biomolecular Engineering; ‡Nebraska Center for Materials and Nanoscience; University of Nebraska-Lincoln, NE 68588, United States

Table of Content Figure

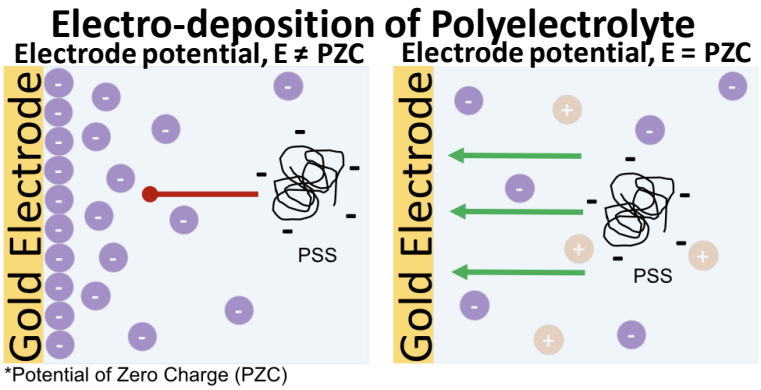

Electrochemical Deposition of Polyelectrolytes is Maximum at the Potential of Zero Charge

David Moore, [†,§] *Jennifer A. Arcila,* [†,§] *Ravi F. Saraf* *[†‡]

†Department of Chemical and Biomolecular Engineering; ‡Nebraska Center for Materials and Nanoscience; University of Nebraska-Lincoln, NE 68588, United States

§ these authors contributed equally

KEYWORDS: Layer-by-layer; polyelectrolyte deposition; electrical double layer; electro-deposition; potential of zero charge

ABSTRACT: Electrochemical deposition of cationic and anionic polyelectrolyte on Au electrode is studied as a function of applied potential between the electrode and the solution of monovalent electrolyte. The deposition is measured by open circuit potential relative to pristine electrode in a reference solution (100 mM NaCl). The rate of deposition is measured by a home-built electrochemical-optical method in real time. It was discovered, that the polarity of the potential or magnitude of potential are not the primary reason to enhance deposition. For example, both the amount and rate of deposition of negatively charged poly(styrene sulfonate) in NaCl is higher when the electrode is at -200 mV than +200 mV with respect to the solution. The results are explained in terms of the charge state of electrical double layer that is primarily controlled by supporting (small) ions.

INTRODUCTION

The polyelectrolyte (PE) thin film on an electrode has a range of modern day applications, such as biosensors[1,2] and energy storage devices.[3-5] The system is highly facile because of a simple immersion coating process which forms a monolayer that can be extended to a complex, stratified, layer-by-layer structure of cationic and anionic polymers[6] due to spontaneous overcharging during PE deposition.[7,8] The modulation of electrostatics by regulating environmental conditions, such as pH, counterion strength, surface charge density, weak versus strong charging of the polymer, and polymer flexibility, to tailor deposition has been exhaustively explored, both experimentally [9,10] and by theory/simulation.[11,12] The layered structure allows the ability to incorporate complexities, such as nanoparticles, mediators, and cofactors in PE thin film. For example, embedding proteins in PE film has led to simple methods for electronically wiring the protein to an underlining electrode for efficient electron transfer. This has led to the development of biosensors,[1,13-15] enzyme fuel cells,[16,17] and the ability to conduct a fundamental study on the charge transport mechanisms by directly coupling the protein to an electrode (i.e., protein voltammetry)[18-23]. Embedding metallic nanoparticles to facilitate electron transport in ion-conducting PE film has led to variety of electrochemical sensors,[24-29] electrocatalytic films,[30] and electronic devices.[31-35]

Electrodeposition of PE by applying a potential, that has been utilized for applications such as anticorrosion coatings decades ago,[36,37] is relatively less explored. The prevalent approach for electrodeposition is to alter the interfacial environment by an active redox reaction to cause polymer precipitation (close to the interface) followed by electrophoretic deposition. Recently, the old process of pH-mediated deposition by hydrolysis[36,37] has been extended to deposit a plethora of PEs, enzymes, cofactors, mediators, and biopolymers for applications such as

biosensors.[38-42] However, the biases are well above 1 V. Using the idea of modulating solubility by redox reaction of the counter ion has been leveraged to achieve electrodeposition at a potential below 1 V without water hydrolysis.[43-46] The active process of redox has also been demonstrated to obtain covalent bond deposition by click chemistry.[47]

The effect of passive (i.e., non-redox) modulation of the interfacial environment on electrodeposition has not been well studied. One primary reason for this is the strong screening of the emanating electric field from the electrode due to the electrical double layer (EDL).[48] Consequently, deposition can be enhanced by invoking a redox reaction to de-screen the EDL by way of rapid electron exchange with the electrode compared to ion diffusion. The process of de-screening was demonstrated by enhancing the amount of binding of target single stranded DNA (ssDNA) in solution to immobilized complimentary probe ssDNA by three orders of magnitude using redox of $[Fe(CN)_6]^{4-/3-}$ in <30 min compared to 8 hrs for simple diffusion limited process.[49]

Here we describe our study on electrodeposition of poly(styrene sulfonate) (PSS) and poly(allylamine hydrochloride) (PAH) on an Au electrode as a self-organization process (rather than self-assembly),[50] where the external potential, *E*, between the electrode and the solution forces the system away from equilibrium to cause ordering (i.e., PE deposition). For the study, we added ~100 mM of NaCl or NaBr to nominally fix the EDL thickness to ~ 5 nm (i.e., Debye length to ~1 nm) and modulate the effective thickness by charging/discharging the EDL by external potential. The driving force for electro-deposition of the PE due to the external potential given by the difference in Fermi level of the electrode and solution are in 100 meV or ~4kT range (where k is Boltzmann's constant and T is temperature of ~300 K). We probed irreversible deposition by open circuit potential and measured rate of deposition in real time

using a home-built differential reflectometer. We specifically studied the role of supporting salts NaCl and NaBr on the deposition of PSS and PAH on Au electrode.

EXPERIMENTAL

Polyelectrolyte Solution Preparation. PSS (Mw = 500 000 Daltons) was obtain from Scientific Polymer Products; and PAH (Mw = 120 000 Daltons), Sodium Chloride (NaCl) ≥ 99.0% and Sodium Bromide (NaBr) ≥ 99.0% were obtained from the Sigma Aldrich Chemical Co. The polydispersity index provided by the supplier was 1.1 to 1.5. De-ionized water of 18 MΩ resistivity was used to prepare all solutions. Aqueous solutions of PSS 10 mM and PAH 10 mM (based on moles of repeat units) were prepared either with 100 mM NaCl or 100 mM NaBr.

Electrode Preparation on Si Chip. Samples were prepared on a 1 cm square Si chip with a 6 mm square Au electrode of ~81 nm roughness and a 1 mm square pad at a corner to provide connection to the electrode (Supporting Information (SI), Section S1). The multilayer electrodes were Au (100 nm)/Ti (70 nm)/SiO2 (5000 nm)/Si substrate. A 5 mm square was patterned on the electrode by photolithography on a 300 nm thick spin casted SU8-2025 photoresist (Microchem). Before each experiment, the chip was exposed to RF plasma (Nordson March Model PX-250) at 38 W and 13.56 MHz for 30 s in O_2 at 70 mTorr to clean the Au electrode surface.

Polyelectrolyte Absorption. After plasma cleaning, the chip was immediately immersed in 10 mM of PAH or PSS with 100 mM NaBr or NaCl. A constant potential (E_{dep}) between the (working/sample) electrode and the reference electrode (Ag/AgCl) in the solution was applied using a potentiostat (Metrohm Autolab). Current between the electrode and a Pt wire counter electrode was measured to monitor the deposition in real-time to determine the integrity of the process (SI, Figure S2).

Measurements of Open Circuit Potential (OCP), V_O. The OCP was measured in 100 mM NaCl at a pH of 6.8 (reference solution). Voltage between the Ag/AgCl reference and the working electrode was measured by a multimeter (Agilent 3458A). The potential reported is of the Au electrode with respect to the solution. To obtain stable measurements, each sample was placed in the reference solution for three hours to reach equilibrium followed by immediate rinse with 100 mM NaCl followed by immersion in freshly made reference solution. (SI, Figure S3 compares the behavior with and without the (optimized) three hour process prior to OCP measurement). Long exposure to reference solution improved reproducibility (SI, Figure S3b). Thus, all the open circuit potentials reported are with respect to the (fresh) reference solution. The analog potential was measured and averaged every 10 s as a function of deposition time, t_{dep} (see typical behavior, SI, Figure S3b). The rate of change of the potential was calculated from the successive averages. The measurement was terminated when the absolute value of the rate of change of the potential remained below 0.1 μV/s for more than 2 min (SI, Figure S3b) to obtain the OCP potential, V_O.

Measurement of Potential of Zero Charge (PZC), V_Z. Measurements of V_Z were performed by a home built electrochemical-optical method.[51] Briefly, the chip was placed in a sealed chamber (of volume ~1 mL) where the patterned electrode was exposed to a solution and the electrical connection was via the peripheral connecting pad outside the chamber. The optical measurement was performed during cyclic voltammetry (CV) using a potentiostat (Metrohm Autolab) with Ag/AgCl and Pt wire as reference and counter electrodes, respectively (SI, Figure S4). The chamber had a transparent window to facilitate optical measurements using a laser beam. The working electrode potential, E, was ramped form -0.2 V to 0.5 V relative to the reference electrode at 100 mV/s. A periodic AC potential of frequency of $\omega = 200$ Hz and an

amplitude of 200 mV peak-to-peak was superimposed on the CV potential, E. The measured reflection is composed of a DC signal corresponding to the incident light intensity Ro, and an AC signal of amplitude R_A due to the oscillation in ions at the electrode interface caused by the applied AC potential. The AC signal was measured using a lock-in amplifier (Signal Recovery 7265 DSP) tuned at ω to obtain differential reflectivity, $R(\omega) = R_A/Ro$. At E equal to V_Z, the R will peak at maximum penetration of the electric field from the electrode due to de-screening by the EDL (SI, Section S4).[52,53] The ω and amplitude are chosen such that $R(2\omega)/R(\omega) < 10^{-3}$. The V_Z is calculated as the formal potential between the peaks at E during forward (V_f) and reverse (V_r) ramps, i.e., $V_Z = (V_f + V_r)/2$. The PE solutions V_Z were measured within a minute after injecting the solution in the chamber to avoid significant polymer deposition on the working electrode. The differential reflectivity is based on local charge in the EDL.[53,54] In principle, as the laser spot can be scanned over the electrode; the instrument is referred to as, Scanning Electrometer for Electrical Double layer (SEED).

Deposition Rate by SEED. Real-time deposition of PE on the (chip) electrode was measured by SEED. The chamber was filled with same solution of PSS or PAH as for V_Z measurements above. The E_{dep} was held constant by the potentiostat and R was measured for 10 min during deposition. The change in differential reflectivity over time was recorded. The rate of change of R with time was measured to obtain relative deposition rate. SEED was on immediately after injecting the solution into the chamber to capture the initial stages of deposition.

RESULTS AND DISCUSSION

The two central properties of interest for this study are OCP and PZC. The OCP, V_O between the electrode and the electrolyte occurs due accumulation of ions at the interface to bring the

electrochemical potentials of the (bulk) electrolyte and the electrode into equilibrium. The result is formation of the EDL. As the Fermi level of Au (relative to vacuum level) is lower than that of the solution, on contact, EDL is negatively charged (i.e., anions are accumulated). Consequently, for pristine Au in non-adsorbing electrolyte solution, applying an external (negative) potential will discharge the EDL. This potential of zero charge, V_Z is nominally equal to $-V_O$. The relationship is not exact due to complexities, such as, finite thickness of EDL that has an exponential charge distribution. As PE binds at multiple sites, the system is forced far from equilibrium by absorbing the polymer due to external potential. As a result, the measured V_O will depart from equilibrium value depending on the amount of polymer adoptions.

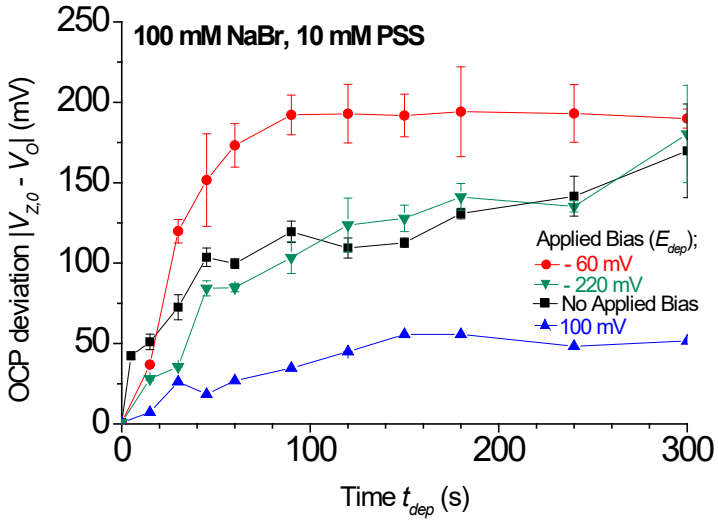

Figure 1. Deposition of PSS in NaBr on Au electrode. Change in $|V_{Z,0} - V_O|$ due to deposition of PSS at different E_{dep} and t_{dep} measured in standard solution (100 mM NaCl).

As the Au electrode was immersed in a solution of PE and salt and a potential E_{dep} was applied, the polymer adsorbed on the electrode which led to change in V_O (relative to V_O for pristine Au in reference solution, $V_{Z,0}$) as t_{dep} increased (Figure 1). To note is that each data point on Figure 1 is a different sample corresponding to deposition conditions, t_{dep} and E_{dep}. The error

bar was based on multiple samples for each condition. As PE deposits on the electrode the OCP deviates from $V_{Z,0}$ (the OCP for pristine Au). There is a sharp initial rise followed by a local plateau. Ignoring the last data point at 300 s for E_{dep} = -220 and 0 mV, $|V_{Z,0} - V_O|$ is reasonably constant for t_{dep} ranging from 100 to 200 s with significant differences between the applied bias, E_{dep}. Thus, to evaluate the effectiveness of electro-deposition we consider the value $|V_{Z,0} - V_O|$ at t_{dep} = 120 s as $|V_{Z,0} - V_O|_P$ at various E_{dep}. Interestingly, $|V_{Z,0} - V_O|_P$ with respect to E_{dep} is not monotonic, i.e., larger external potential does not proportionally increase the amount of ultimate deposition of PE due to the potential. As noted above, the process is shifted from equilibrium, i.e., self-organization rather than self-assembly.[50] Due to polymer adsorption V_O departs from $V_{Z,0}$ due to the added charge on the surface. If we assume that the mole fraction of (partial) charge compensation on the polymer due to counter ion (Na^+ for PSS and Cl^- for PAH) is constant, then $|V_{Z,0} - V_O|$ is linearly proportional to the amount of PE deposition. The assumption is reasonable, as the deposition is at most few monolayers, as indirectly inferred from PZC measurements discussed below (Figure 3).

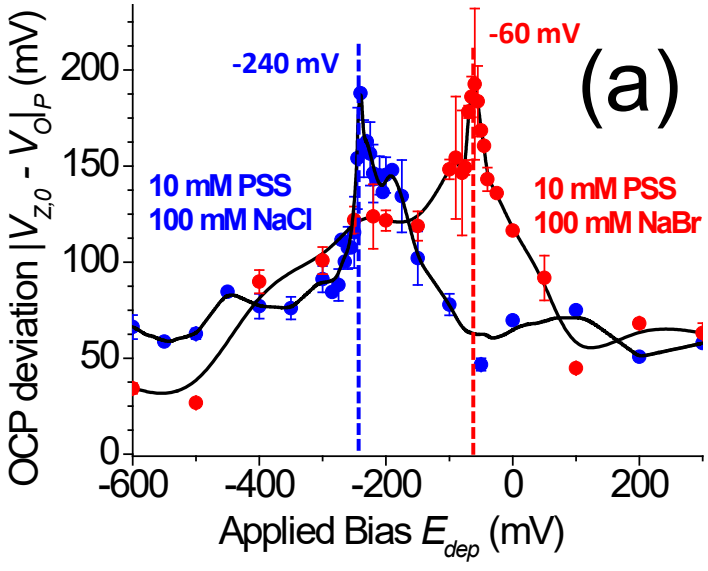

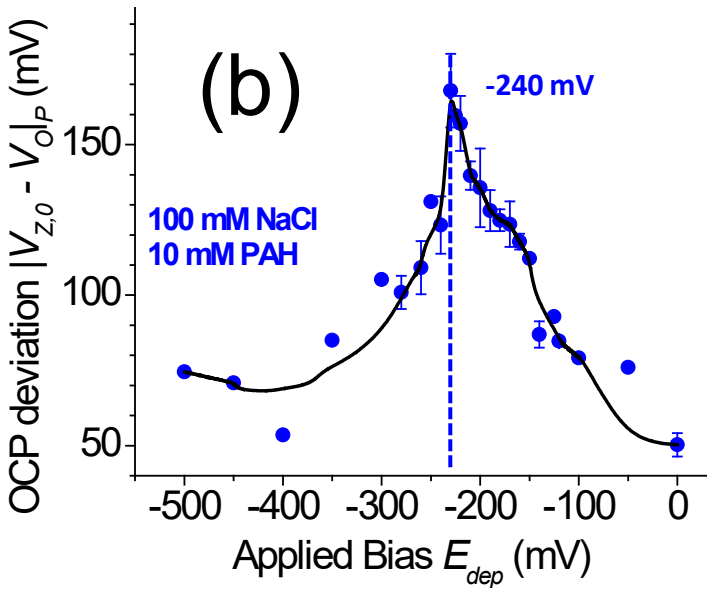

Figure 2. Deposition of PE on Au electrode measured by OCP deviation at different E_{dep}. (a) Deposition of PSS with maxima close to PZC of the corresponding salt in solution. (b) Deposition of PAH with maximum close to PZC of NaCl.

From the above assumption of constant charge density of adsorbed film, the deviation from $V_{Z,0}$, $(|V_{Z,0} - V_O|_P)$ is equal to the relative change in the thickness of PE due to electro-deposition as a function of E_{dep} (Figure 2). For PSS in NaCl and NaBr the maximum deposition occurred at -240 mV and -60 mV, respectively (Figure 2a). For PAH in NaCl, the maximum deposition is at -240 mV, similar to PSS in NaCl (Figure 2b). The peaks were prominently sharp and significantly shifted for different electrolytes. The E_{dep} for maximum deposition primarily depended on Cl^- versus Br^- in the electrolyte rather than the sign of the charge on the PE. The enhancement in thickness at PZC may be estimated as follows: Typically, the (saturated) thickness for the first layer of PSS and PAH deposition on Au in NaCl in quiescent conditions (i.e., E_{dep} = 0 V) is approximately 1.5 nm and 1 nm for PSS and PAH, respectively.[55] The deposition at PZC is enhanced by ~3 fold and 1.8 fold for PSS (Fig. 2(a) and PAH (Fig. 2(a)), respectively, relative to

E_{dep} = 0. Thus, the thickness at PZC for PSS and PAH is ~4.5 nm and ~2 nm, respectively. We note in passing that overnight deposition at PZC and 0 V had <25 mV change in OCP indicating the estimated values are nominally at saturation. The characteristics for PAH in NaBr are not reported because of its anomalous behavior as will be discussed below in terms of the PZC characteristics (Figure 3b).

As the magnitudes of V_O and V_Z are nominally similar, we consider the PZC of PE modified electrode. The V_Z was measured by SEED (see Experimental Section and SI Section S4). In the CV during SEED, when the potential is around the PZC the EDL is discharged. As a result, the electric field from the electrode emanates deeper in the solution to cause significant increase in ion oscillation due to the (small) AC potential superimposed on the CV ramp. The SEED measures a peak in amplitude of ion oscillation as a maxim in differential reflectivity signal, R when the CV potential, E (= V_Z) is at the PZC (Figure 3). Thus, PZC is measured directly. The "halo" around each curve was obtained by averaging over 10 CV cycles (see SI, Figure S5). For NaCl with PSS or PAH in the solution the V_Z on Au is nominally similar to pure electrolyte (Figure 3a). This indicates that the charge compensation is primarily due to the Cl^- (as the EDL of gold is negatively charged). There is larger shift of ~30 mV for PSS while virtually no shift occurs for PAH (i.e., within 10 mV which is instrument sensitivity for CV). The latter is expected as PAH will not interact with Au (that tends to attract anions). While for PSS the V_Z shifts to lower magnitude indicating some adsorption of the polymer. For NaBr, addition of PSS does not show significant effect as above (Figure 3b). However, for PAH the shift in V_Z is over 300 mV. Furthermore, the sign changes and the R is asymmetric. The anomalous behavior is under investigation and will not be reported here. A possible explanation is briefly discussed in Section S7 in SI. Importantly, E_{dep} for maximum deposition signified by the peaks in $|V_{Z,0} - V_O|_P$

(Figure 2) and the V_Z for the same system (Figure 3) are nominally equal in magnitude indicating that, maximum enhancement in deposition due to electric field is when E_{dep} discharges the EDL.

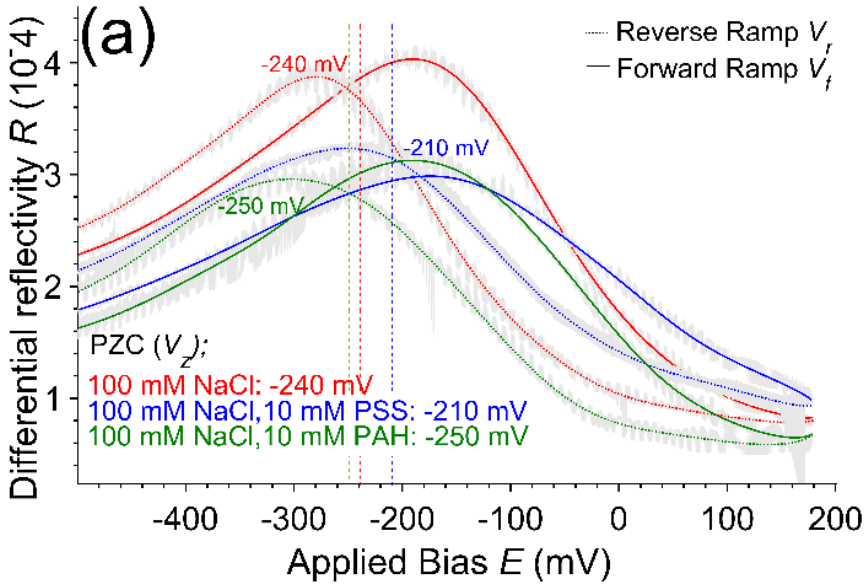

Figure 3. Measurement of PZC by SEED. Differential reflectivity during CV ramp on pristine Au right before PE deposition. The PZC is average potential of forward and reverse peaks. (a) PZC of solutions containing 100mM NaCl. (b) PZC of solutions containing 100mM NaBr.

The two methods of measuring OCP and PZC are significantly different. OCP was based on end-point of adsorption while PZC was based on solution property with minimal deposition. The remarkable concurrence between these two orthogonal approaches indirectly supports that the sample preparations approach to measure OCP (particularly the stabilization process of immersion for three hours in reference solution) is reasonable. Furthermore, the deposition of PE on Au is at most only a few monolayers, otherwise the E_{dep} for maximum deposition would significantly depart from the V_Z of the solution.

Next, we consider the rate of deposition as measured by SEED. Similar to OCP experiment, the PE is deposited at fixed $E = E_{dep}$ and R was measured over a period of 10 min. The differential reflectivity, R, decreased monotonically over time for all the three solution (SI, Figure S6a-c). The decrease in R was attributed to the screening of the electric field emanating from the electrode due to PE deposition. For solutions without the PE the R was stable confirming that the decrease is indeed due to polymer deposition (SI, Figure S6d,e). The change in R was nominally linear leading to a constant slope, S. From Guass' law, the screening of the electric field is proportional to the charge deposited. Assuming the charge density of the PE deposited is constant, the decrease in R is nominally proportional the PE thickness deposited. Again, assuming mole fraction of compensating charge on PE is constant; the slope is proportional to the rate of PE deposition. Similar to total amount of deposition measured by $|V_{Z,0} - V_O|_P$ (Figure 2), $|S|$ was maximum at V_Z (Figure 4)). To ensure that S is exclusively due to polymer deposition, no peak is observed without the polymer (SI, Figure S7). Thus, both the amount and rate of deposition is highest at the PZC.

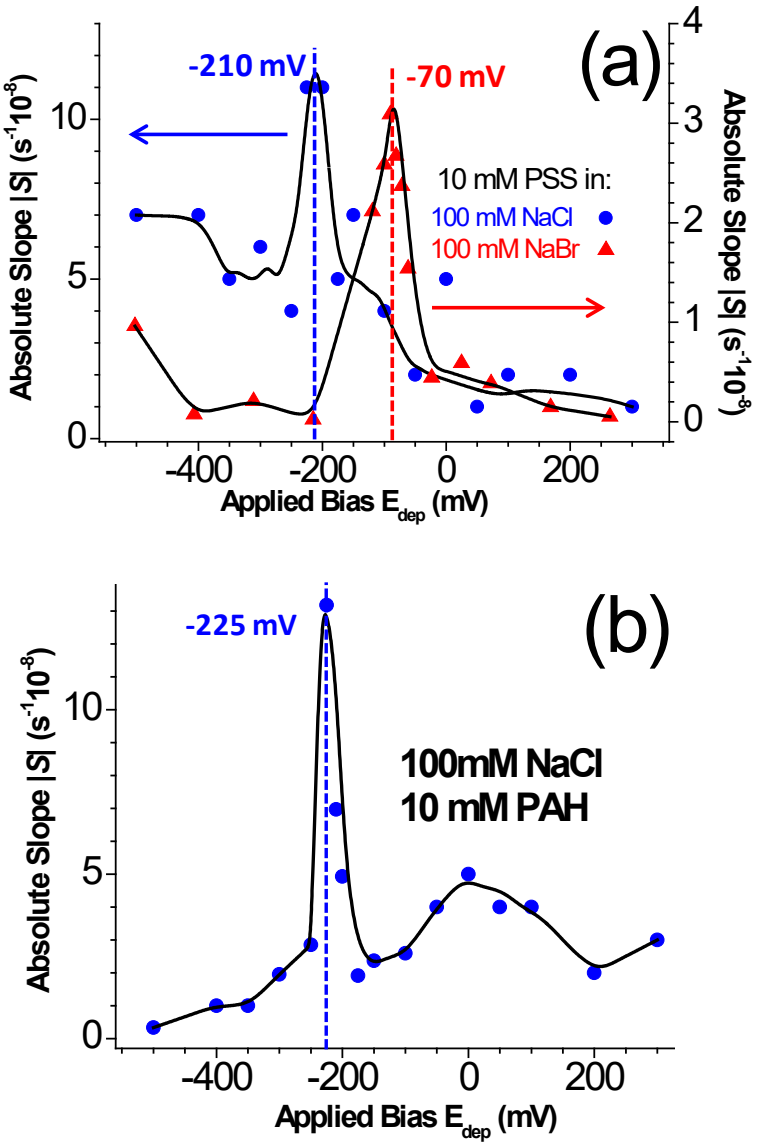

Figure 4. Rate of PE deposition measured by SEED. Differential reflectivity during deposition reduces linearly at a fixed E_{dep} due to PE deposition (SI, Fig. S6) with a slope, S. The magnitude of S as a function of E_{dep} peaks depends on the PE and the electrolyte. (a) Deposition rate of PSS with maximum close to PZC of the corresponding salt in solution. (b) Deposition rate of PAH with maximum close to PZC of NaCl.

The observation of maximum deposition at E_{dep} coinciding with V_Z and the importance of electrolyte were examined. We considered the relative Fermi levels of the electrode and solution

rather than electrochemical potentials for convenience. (As the discussion is relative, absolute levels are not relevant). Let's take the solution as reference ground. As the Au electrode is immersed in PE solution, anions will be attracted towards the electrode because the Fermi level of Au is lower than that of solution. Owing to the higher mobility of Cl^- or Br^-, the smaller ions will diffuse over an order of magnitude faster than PSS towards the surface to form the EDL. (PAH, when present will be repelled). As the potential of the electrode in made more positive, i.e., Fermi level of electrode goes down, the smaller anions will diffuse faster towards the electrode to screen the field to further reduce the driving force for PSS to be attracted. When the potential is made negative, i.e., Fermi level goes up, beyond PZC, the same dynamics will apply for Na^+ in PAH solution, where the former will outpace the latter. However, when the Fermi level aligns with PZC, the EDL is completely discharged and the field emanates the farthest. In this situation all the ions (positive and negative, small ions and PE), are attracted towards the electrode due to image charge. The Columbic attraction on PE (PSS or PAH) is orders of magnitude larger than the thermal energy unlike with the smaller ions. Furthermore, due to multiple binding sites in the polymer, it is difficult for PE (PSS or PAH) to detach (by thermal motion) from the surface once adsorbed. Thus, the polymer will adsorb and make the system off-equilibrium leading to a finite deviation of OCP, i.e., $|V_Z - V_{Z,0}| > 0$.

CONCLUSIONS

We studied the electrodeposition process of negatively and positively charged polymers, PSS and PAH, respectively, on Au surface. Electrodeposition was achieved by applying a potential (E_{dep}) between the Au electrode and the solution of 10 mM polymer in 100 mM of NaCl or NaBr. The process was characterized by measuring the OCP for different deposition time (t_{dep}), and the rate of deposition was measured by differential reflectivity using a home built

instrument. Deposition was achieved within t_{dep} of five minutes as manifested by leveling of OCP. The real time deposition by differential reflectivity showed a constant rate for 10 min for exposure to E_{dep}. The results indicated that both the amount and rate of deposition is highest when E_{dep} is close to the PZC of the solution which is determined by the small ions (primarily, Cl^- and Br^- because the EDL of Au is negatively charged). The implication appears counter-intuitive. For example, the deposition of PSS in NaCl was higher when the electrode was at -200 mV relative to the solution rather than +200 mV; and larger external potentials do not favor electrodeposition beyond to the PZC of the solution. Our results differ with previous reports that indicate that charge deposition/attraction in PE systems is possible only in the presence of multivalent ions[56-59]. As the deposition is remarkably sharp around the PZC of the solution, the approach may potentially have applications in developing complex nanoscale architectures by modulating working function of the electrodes and local PZC of the solution/electrode system.

ASSOCIATED CONTENT

Supporting Information. Detailed description of chip fabrication; Determination of polymer deposition end-point; Explanation of required equilibrium time for OCP measurements; SEED set-up and principle of PZC measurements; Raw data for polymer deposition rate; Controls for Figure 4 showing no peak for solution without PE. A table summarizing the measured PZC and maximum potential for PE deposition amount and deposition rate.

AUTHOR INFORMATION

Corresponding Author

*E-mail: rsaraf2@unl.edu

Author Contributions

The manuscript was written through contributions of all authors. All authors have given approval to the final version of the manuscript. § These authors contributed equally.

Funding Sources

R.F.S. would like to thank the NSF (CBET-1353125) for financial support.

ABBREVIATIONS

PE, Polyelectrolyte; EDL, electrical double layer; PSS, poly(styrene sulfonate); PAH, poly(allylamine hydrochloride); OCP, open circuit potential method; $V_{O,}$ open circuit potential magnitude; PZC, potential of zero charge method; $V_{Z,}$ potential of zero charge magnitude; V_f, potential of maximum peak height for forward ramps; $V_{r,}$ potential of maximum peak height for reverse ramps; $V_{Z,0}$, potential of zero charge of gold immersed in 100 mM NaCl; CV, cyclic voltammetry; SEED, Scanning Electrometer for Electrical Double layer; $t_{dep,}$ polymer deposition time; E_{dep}, constant potential for polymer deposition; E, applied potential during CV; Ro, incident light intensity; $R_{A,}$ AC signal amplitude due to the oscillation in ions at the electrode interface; R, differential reflectivity unit;

REFERENCES

1. Zheng, L. Z.; Yao, X.; Li, J. H. Layer-by-layer assembly films and their applications in electroanalytical chemistry. Current Analytical Chemistry 2006, 2 (3), 279-296.

2. Skorb, E. V.; Volkova, A. V.; Andreeva, D. V. Layer-by-Layer Approach for Design of Chemical Sensors and Biosensors. Current Organic Chemistry 2015, 19 (12), 1097-1116.

3. Christinelli, W. A.; Goncalves, R.; Pereira, E. C. A new generation of electrochemical supercapacitors based on layer-by-layer polymer films. Journal of Power Sources 2016, 303, 73-80.

4. Nystrom, G.; Marais, A.; Karabulut, E.; Wagberg, L.; Cui, Y.; Hamedi, M. M. Self-assembled three-dimensional and compressible interdigitated thin-film supercapacitors and batteries. Nature Communications 2015, 6.

5. Wang, J. A.; Lu, Y. T.; Lin, S. C.; Wang, Y. S.; Ma, C. C. M.; Hu, C. C. Designing a Novel Polymer Electrolyte for Improving the Electrode/Electrolyte Interface in Flexible All-Solid-State Electrical Double-Layer Capacitors. Acs Applied Materials & Interfaces 2018, 10 (21), 17871-17882.

6. Decher, G. Fuzzy nanoassemblies: Toward layered polymeric multicomposites. Science 1997, 277 (5330), 1232-1237.

7. Ladam, G.; Schaad, P.; Voegel, J. C.; Schaaf, P.; Decher, G.; Cuisinier, F. In situ determination of the structural properties of initially deposited polyelectrolyte multilayers. Langmuir 2000, 16 (3), 1249-1255.

8. Grosberg, A. Y.; Nguyen, T. T.; Shklovskii, B. I. Colloquium: The physics of charge inversion in chemical and biological systems. Reviews of Modern Physics 2002, 74 (2), 329-345.

9. Borges, J.; Mano, J. F. Molecular Interactions Driving the Layer-by-Layer Assembly of Multilayers. Chemical Reviews 2014, 114 (18), 8883-8942.

10. Richardson, J. J.; Cui, J. W.; Bjornmalm, M.; Braunger, J. A.; Ejima, H.; Caruso, F. Innovation in Layer-by-Layer Assembly. Chemical Reviews 2016, 116 (23), 14828-14867.

11. Faraudo, J.; Martin-Molina, A. Competing forces in the interaction of polyelectrolytes with charged interfaces. Current Opinion in Colloid & Interface Science 2013, 18 (6), 517-523.

12. Rydzek, G.; Ji, Q. M.; Li, M.; Schaaf, P.; Hill, J. P.; Boulmedais, F.; Ariga, K. Electrochemical nanoarchitectonics and layer-by-layer assembly: From basics to future. Nano Today 2015, 10 (2), 138-167.

13. Giustini, M.; Autullo, M.; Mennuni, M.; Palazzo, G.; Mallardi, A. Polymer-photosynthetic protein multilayer architectures for herbicide optical detection. Sensors and Actuators B-Chemical 2012, 163 (1), 69-75.

14. Yu, X.; Sotzing, G. A.; Papadimitrakopoulos, F.; Rusling, J. F. Wiring of enzymes to electrodes by ultrathin conductive polyion underlayers: Enhanced catalytic response to hydrogen peroxide. Analytical Chemistry 2003, 75 (17), 4565-4571.

15. Aghamiri, Z. S.; Mohsennia, M.; Rafiee-Pour, H. A. Immobilization of cytochrome c and its application as electrochemical biosensors. Talanta 2018, 176, 195-207.

16. Perveen, R.; Inamuddin; Nasar, A.; Beenish; Asiri, A. M. Synthesis and characterization of a novel electron conducting biocomposite as biofuel cell anode. International Journal of Biological Macromolecules 2018, 106, 755-762.

17. Noll, T.; Noll, G. Strategies for "wiring" redox-active proteins to electrodes and applications in biosensors, biofuel cells, and nanotechnology. Chemical Society Reviews 2011, 40 (7), 3564-3576.

18. Kong, J. L.; Lu, Z. Q.; Lvov, Y. M.; Desamero, R. Z. B.; Frank, H. A.; Rusling, J. F. Direct electrochemistry of cofactor redox sites in a bacterial photosynthetic reaction center protein. Journal of the American Chemical Society 1998, 120 (29), 7371-7372.

19. Takahashi, S.; Watahiki, R.; Tomida, K.; Wang, B. Z.; Anzai, J. Voltammetric Studies on Gold Electrodes Coated with Chitosan-Containing Layer-by-Layer Films. Materials 2013, 6 (11), 5427-5439.

20. Duff, J. L. C.; Breton, J. L. J.; Butt, J. N.; Armstrong, F. A.; Thomson, A. J. Novel redox chemistry of [3Fe-4S] clusters: Electrochemical characterization of the all-Fe(II) form of the [3Fe-4S] cluster generated reversibly in various proteins and its

spectroscopic investigation in Sulfolobus acidocaldarius ferredoxin. Journal of the American Chemical Society 1996, 118 (36), 8593-8603.

21. Feng, J. J.; Zhao, G.; Xu, J. J.; Chen, H. Y. Direct electrochemistry and electrocatalysis of heme proteins immobilized on gold nanoparticles stabilized by chitosan. Analytical Biochemistry 2005, 342 (2), 280-286.

22. Beissenhirtz, M. K.; Kafka, B.; Schafer, D.; Wolny, M.; Lisdat, F. Electrochemical quartz crystal microbalance studies on cytochrome c/polyelectrolyte multilayer assemblies on gold electrodes. Electroanalysis 2005, 17 (21), 1931-1937.

23. Wettstein, C.; Mohwald, H.; Lisdat, F. Coupling of pyrroloquinoline quinone dependent glucose dehydrogenase to (cytochrome c/DNA)-multilayer systems on electrodes. Bioelectrochemistry 2012, 88, 97-102.

24. Calaca, G. N.; Erdmann, C. A.; Soares, A. L.; Pessoa, C. A.; Fujiwara, S. T.; Garcia, J. R.; Vidotti, M.; Wohnrath, K. Layer-by-Layer AuNPs-SiPy+/Prussian blue nanoparticles modified electrodes: characterization and electrocatalytic effects. Electrochimica Acta 2017, 249, 104-112.

25. Barsan, M. M.; Brett, C. M. Recent advances in layer-by-layer strategies for biosensors incorporating metal nanoparticles. Trac-Trends in Analytical Chemistry 2016, 79, 286-296.

26. Crespilho, F. N.; Zucolotto, V.; Oliveira, O. N.; Nart, F. C. Electrochemistry of Layer-by-Layer Films: a review. International Journal of Electrochemical Science 2006, 1 (5), 194-214.

27. dos Santos, V.; de Jesus, C. G.; dos Santos, M.; Canestraro, C. D.; Zucolotto, V.; Fujiwara, S. T.; Garcia, J. R.; Pessoa, C. A.; Wohnrath, K. Platinum nanoparticles incorporated in silsesquioxane for use in LbL films for the simultaneous detection of dopamine and ascorbic acid. Journal of Nanoparticle Research 2012, 14 (9).

28. Iost, R. M.; Crespilho, F. N. Layer-by-layer self-assembly and electrochemistry: Applications in biosensing and bioelectronics. Biosensors & Bioelectronics 2012, 31 (1), 1-10.

29. Liu, Y.; Cui, T. H. Ion-sensitive field-effect transistor based pH sensors using nano self-assembled polyelectrolyte/nanoparticle multilayer films. Sensors and Actuators B-Chemical 2007, 123 (1), 148-152.

30. Li, H.; Jia, L. P.; Ma, R. N.; Jia, W. L.; Wang, H. S. Electrodeposition of PtNPs on the LBL assembled multilayer films of (PDDA-GS/PEDOT:PSS)(n) and their electrocatalytic activity toward methanol oxidation. Rsc Advances 2017, 7 (27), 16371-16378.

31. Kumlangdudsana, P.; Tuantranont, A.; Dubas, S. T.; Dubas, L. Fabrication of microelectrodes using flow layer-by-layer self assembly of gold nanoparticles. Superlattices and Microstructures 2012, 52 (5), 1043-1051.

32. Cheng, W. L.; Campolongo, M. J.; Tan, S. J.; Luo, D. Freestanding ultrathin nano-membranes via self-assembly. Nano Today 2009, 4 (6), 482-493.

33. Promnimit, S.; Jafri, S. H. M.; Sweatman, D.; Dutta, J. Conduction Properties of Layer-by-Layer Self-Assembled Multilayer Nanoparticulate Structures. Journal of Nanoelectronics and Optoelectronics 2008, 3 (2), 184-189.

34. Maheshwari, V.; Saraf, R. F. High-resolution thin-film device to sense texture by touch. Science 2006, 312 (5779), 1501-1504.

35. Nguyen, C. V.; Saraf', R. F. Tactile Imaging of an Imbedded Palpable Structure for Breast Cancer Screening. Acs Applied Materials & Interfaces 2014, 6 (18), 16368-16374.

36. Brewer, G. E. F. Electrophoretic Painting. Journal of Applied Electrochemistry 1983, 13 (3), 269-275.

37. Hope, P. Electrophoretic painting - the way forward. Anti-Corrosion Methods and Materials 1998, 45 (3), 146-+.

38. Wu, L. Q.; Gadre, A. P.; Yi, H. M.; Kastantin, M. J.; Rubloff, G. W.; Bentley, W. E.; Payne, G. F.; Ghodssi, R. Voltage-dependent assembly of the polysaccharide chitosan onto an electrode surface. Langmuir 2002, 18 (22), 8620-8625.

39. Wang, Y.; Pang, X.; Zhitomirsky, I. Electrophoretic deposition of chiral polymers and composites. Colloids and Surfaces B-Biointerfaces 2011, 87 (2), 505-509.

40. Wu, K. M.; Imin, P.; Sun, Y. C.; Pang, X.; Adronov, A.; Zhitomirsky, I. Electrophoretic deposition of composite films from solutions of conjugated polymers and their supramolecular complexes with carbon nanotubes. Materials Letters 2012, 67 (1), 248-251.

41. Maerten, C.; Jierry, L.; Schaaf, P.; Boulmedais, F. Review of Electrochemically Triggered Macromolecular Film Buildup Processes and Their Biomedical Applications. Acs Applied Materials & Interfaces 2017, 9 (34), 28117-28138.

42. Ngankam, A. P.; Van Tassel, P. R. Continuous polyelectrolyte adsorption under an applied electric potential. Proceedings of the National Academy of Sciences of the United States of America 2007, 104 (4), 1140-1145.

43. Sadman, K.; Wang, Q. F.; Chen, S. H.; Delgado, D. E.; Shull, K. R. pH-Controlled Electrochemical Deposition of Polyelectrolyte Complex Films. Langmuir 2017, 33 (8), 1834-1844.

44. Olsen, C.; Van Tassel, P. R. Polyelectrolyte adsorption kinetics under an applied electric potential: Strongly versus weakly charged polymers. Journal of Colloid and Interface Science 2009, 329 (2), 222-227.

45. Martin, E. J.; Sadman, K.; Shull, K. R. Anodic Electrodeposition of a Cationic Polyelectrolyte in the Presence of Multivalent Anions. Langmuir 2016, 32 (31), 7747-7756.

46. Mergel, O.; Kuhn, P. T.; Schneider, S.; Simon, U.; Plampera, F. A. Influence of Polymer Architecture on the Electrochemical Deposition of Polyelectrolytes. Electrochimica Acta 2017, 232, 98-105.

47. Rydzek, G.; Thomann, J. S.; Ben Ameur, N.; Jierry, L.; Mesini, P.; Ponche, A.; Contal, C.; El Haitami, A. E.; Voegel, J. C.; Senger, B.; Schaaf, P.; Frisch, B.; Boulmedais, F. Polymer Multilayer Films Obtained by Electrochemically Catalyzed Click Chemistry. Langmuir 2010, 26 (4), 2816-2824.

48. Andelman, David & Joanny, Jean-Francois. (2000). Polyelectrolyte Adsorption. Journal De Physique. 49. 10.1016/S1296-2147(00)01130-6.

49. Raghunath, S.; Prasad, A.; Tevatia, R.; Gunther, J. R.; Roy, S.; Krishnan, S.; Saraf, R. F. Quantitative Electrochemical DNA Microarray on a Monolith Electrode with Ten Attomolar Sensitivity, 100% Specificity, and Zero Background. Chemelectrochem 2018, 5 (3), 429-433.

50. Mann, S. Self-assembly and transformation of hybrid nano-objects and nanostructures under equilibrium and non-equilibrium conditions. Nature Materials 2009, 8 (10), 781-792.

51. Yu, C. C.; Lee, S. W.; Ong, J.; Moore, D.; Saraf, R. F. Single Electron Transistor in Aqueous Media. Advanced Materials 2013, 25 (22), 3079-3084.

52. Lee, S. W.; Lopez, J.; Saraf, R. F. Fabrication and Properties of Redox Ion Doped Few Monolayer Thick Polyelectrolyte Film for Electrochemical Biosensors at High Sensitivity and Specificity. Electroanalysis 2013, 25 (6), 1557-1566.

53. Singh, G.; Saraf, R. F. Direct measurement of ion accumulation at the electrode electrolyte interface under an oscillatory electric field. Journal of Physical Chemistry B 2006, 110 (25), 12581-12587.

54. Lee, S. W.; Lopez, J.; Saraf, R. F. Direct mapping of local redox current density on a monolith electrode by laser scanning. Biosensors & Bioelectronics 2013, 47, 408-414.

55. Konopsky V. N.; Karakouz T.; Alieva E. V.; Vicario C.; Sekatskii S. K.; Dietler G. Photonic Crystal Biosensor Based on Optical Surface Waves. Sensors 2013, 13, 2566-2578.

56. Diehl, A.; Carmona, H. A.; Levin, Y. Counterion correlations and attraction between like-charged macromolecules. Physical Review e 2001, 64 (1).

57. GronbechJensen, N.; Mashl, R. J.; Bruinsma, R. F.; Gelbart, W. M. Counterion-induced attraction between rigid polyelectrolytes. Physical Review Letters 1997, 78 (12), 2477-2480.

58. Martin-Molina, A.; Ibarra-Armenta, J. G.; Gonzalez-Tovar, E.; Hidalgo-Alvarez, R.; Quesada-Perez, M. Monte Carlo simulations of the electrical double layer forces in the presence of divalent electrolyte solutions: effect of the ion size. Soft Matter 2011, 7 (4), 1441-1449.

59. Turesson, M.; Labbez, C.; Nonat, A. Calcium Mediated Polyelectrolyte Adsorption on Like-Charged Surfaces. Langmuir 2011, 27 (22), 13572-13581.

Supporting Information

Electrochemical Deposition of Polyelectrolytes is Maximum at the Potential of Zero Charge

David Moore, [†,§] Jennifer A Arcila, [†,§] Ravi F. Saraf[†,‡,*]

[†]Department of Chemical and Biomolecular Engineering, [‡]Nebraska Center for Materials and Nanoscience; University of Nebraska-Lincoln, NE 68512; *rsaraf2@unl.edu

([§] these authors contributed equally)

S1. Chip Fabrication

The 1 cm square Si chip with 5000 nm thick thermal oxide SiO_2, was used to deposit 100 nm thick Au and 70 nm thick Ti as adhesion layer (Figure S1). The deposition of the electrode metals, Au was obtained by RF Sputtering. Using Laser Scanning Microscopy Keyence VK-X200K the resulting surface was characterized with an average roughness (*Ra*) of 81 ± 6 nm, maximum profile peak height (*Rp*) of 303 ± 19 nm and maximum profile valley depth (*Rv*) of 295 ± 13 nm. The chip was cleaned using RF plasma (Nordson March Model PX-250) at 38 W and 13.56 MHz with O_2 at 70 mTorr for 2 min, followed by immersion in Piranha solution (75% Sulfuric Acid and 25% Hydrogen peroxide) to remove organic residues. Standard lithography using SU8 – 2025 as photoresist diluted 1:4 with cyclopentanone was performed to create a 5 mm square pattern. The thickness of resist was 300 nm. For lithography the chip was pre-baked for 45 s at 90 °C followed by exposure to 300 W Xe light for 45 s through a contact mask. The pattern was immersed in SU8 developer (Microchem) to remove the unexposed resist (negative resist). To improve cured SU8 adhesion to the surface the chip was hard baked at 140 °C for 1 hr. The chip was subjected to a final RF plasma cleaning under same conditions as above for 30 s to ensure clean Au electrode surface before polyelectrolyte (PE) deposition.

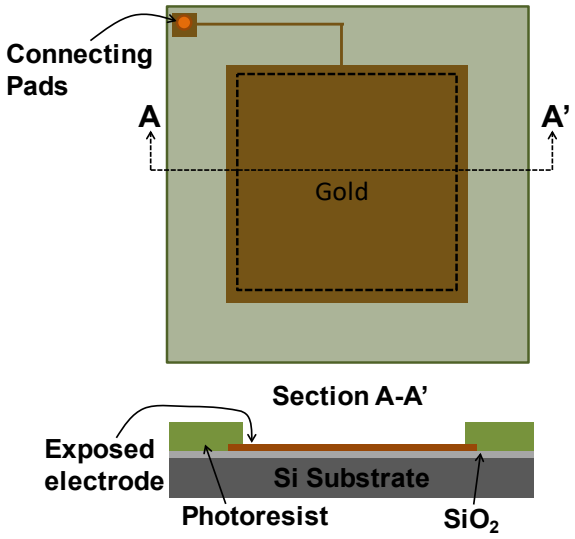

Figure S1. Chip showing the Au electrode with connection pad to the potentiostat for electrochemical experiments.

S2. Real-time monitoring of PE deposition to determine reproducibility

During the deposition step, a current was observed that rapidly reaches saturation (Figure S2a). As the initial charge accumulation occurs primarily due to double layer charging from PE and associated counter ions, a (capacitive) current is generated. We monitor this capacitive current to qualitatively ensure that the deposition process reaches saturation. The current does not decay to zero due to non-idealities, such as the counter and working electrodes not behaving as ideal polarizable electrodes that act as perfect capacitors (e.g. leakage current), and the reference Ag/AgCl electrode is not completely non-polarizable. The long-scale PE deposition was indistinguishable from the electrolytic double layer charging, so calculation of the accumulated PE charge was not possible. However, the test enables us to ensure the reproducibility of the system, i.e., quality of the electrode and electrical circuity including the reference electrode function, or large adsorption or desorption events of impurities or aggregated PE. For example, current jumps during deposition are rejected because they are not reproducible (Figure S2b).

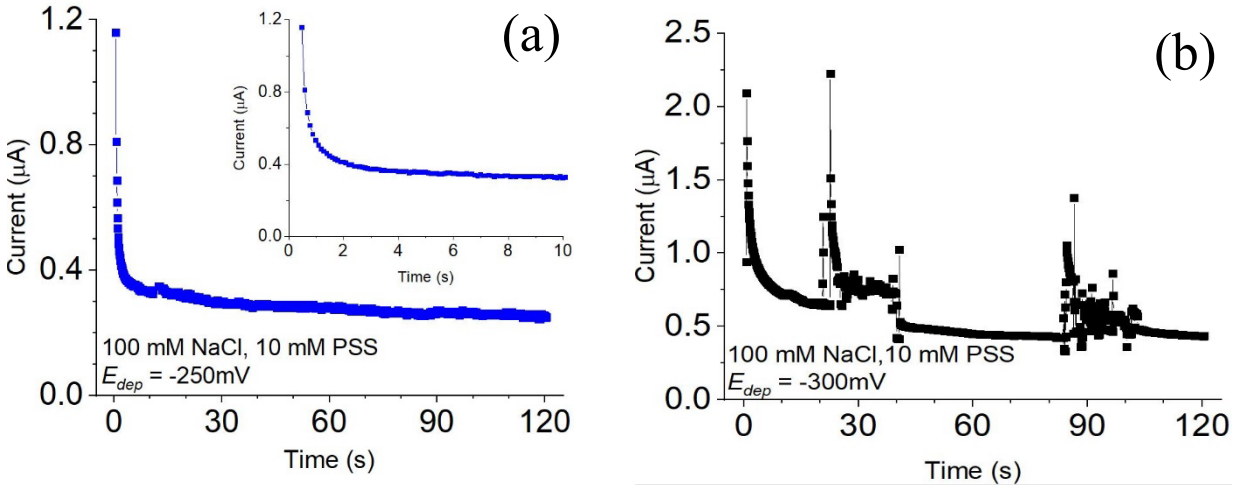

Figure S2. Typical current measured during deposition of PE. (a) Expected current behavior under optimal experimental conditions; Insert correspond to first 10 s of the same experiment. (b) Poorly-behaved current causing the run to be rejected.

S3. Open Circuit Potentials (OCP) measurements

OCP was measured in 100 mM NaCl (reference solution) because both PAH and the reference electrode were potential sources of Cl^- ions, and measuring in different environments affected the results. The OCP measurements were carried out using a the following regiment: Immediately after deposition and a vigorous rinse in DI water of the sample to remove any remaining polyelectrolyte, the sample was placed in reference solution for three hours followed by another rinse in reference solution and immersion in freshly made reference solution to perform the OCP measurement. If no three-hour soaking was performed, the OCP in reference solution for various deposition bias conditions showed undesirable behavior (Figure S3a). For example, the OCP did not plateau for well over an hour (deposition at -300 mV in Figure S3a). The OCP showed anomalous behavior (deposition at -600 mV and 0 mV). In all cases, the initial OCP tended to be near the held potential, indicating an incomplete discharge of the double layer capacitance, which might also suggest excess polyelectrolyte could be loosely bound to the surface. This concern was supported by the observation of "jumps" in some voltage measurements (Figure S3a, -600 mV). Additionally, the long settling time of these runs contributed to measurement error as the end-point may incorrectly defined (i.e., for deposition at 0 mV there is a slow decay of OCP well beyond 1000 s). Reported measurements of OCP were allowed to settle until the potential changes slower than 1 μV per second for the full duration of two minutes. This typically occurred on the order of 600 seconds. The three hours was sufficient to presumably leech the counter ions, desorb excess PE, and perhaps facilitate conformational rearrangement of the PE chain. The success was indicated by smooth potential-time characteristics (Figure S3b).

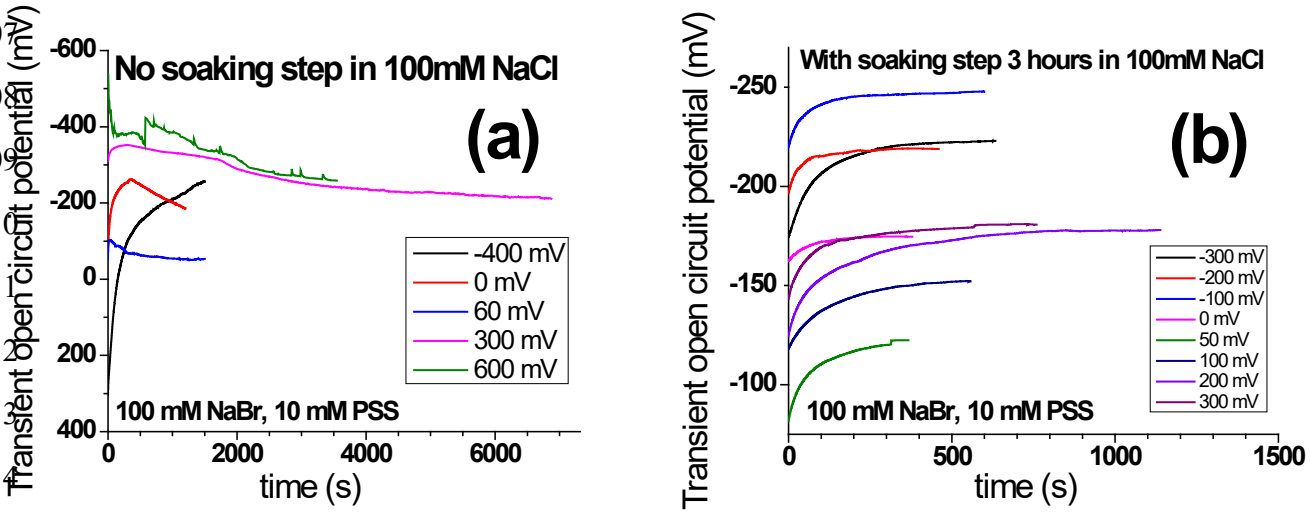

Figure S3. Open circuit potential as a function of time after deposition of PE at E_{dep}, for samples that were (a) not immersed; and (b) immersed, in 100 mM NaCl reference solution prior to the measurement. The curves are for different E_{dep} condition.

S4. Measurement of PZC by SEED

Although SEED has been described earlier[1-4] and its application to measurement of PZC has been shown,[5] here we briefly describe the instrument and the PZC measurement for convenience to the reader.

A 632 nm Helium-Neon (He-Ne) laser is directed to an objective lens using mirrors and beam splitters, where it is focused to a ~6 um spot on the surface of the electrode. The reflected light is then directed to a silicon photodetector using a beam splitter, labeled BS1 in Figure S4. The signal from the photodetector is amplified by a transconductance amplifier and fed to a lock-in amplifier to acquire R_A as well as a data acquisition card connected to a computer to acquire R_O. The differential reflected signal, $R = R_A/R_O$ is calculated and stored in the computer.

The reason for a peak at PZC is as follows. The oscillation of the refractive index occurs due to oscillation in the refractive index caused by the motion of ions due to the AC potential. Say, n_e and n_b are the refractive indices of the electrode and the solution near the electrode, respectively. Then Fresnel's law, at normal incidence, gives the reflectivity r by:[6]

$$r = \frac{n_b - n_e}{n_b + n_e},$$

As the ions near the surface of the electrode oscillate at frequency ω due to the applied AC voltage, the n_b oscillates due to oscillation in ion concentration that is linearly proportional to the differential refractive index of the solution. As a result, the reflectivity oscillation at ω, r_{AC}, is given by (see Tevatia et al., SI, Section S4),[6]

$$r_{AC} = K_1 \frac{dn}{dc} \langle \delta c \rangle cos\omega t$$

where, K_1 is a constant, and dn/dc is differential refractive index of the ions, and $\langle \delta c \rangle$ is the average concentration at the interface[6]. The ion oscillation reaches a local maximum as E approaches the V_Z due to decreased screening of charges. As a result, the differential reflectivity, R shows a peak that is proportional to the amplitude of oscillation of ion concentration averaged over the interface. A typical signal of differential reflectivity over CV cycle shows two peaks in forward and reverse ramps (Figure S5). The signal for each cycle is superimposed (gray halo) and averaged over 10 cycles to obtain the PZC response curves (smooth curves) (Figure 3).

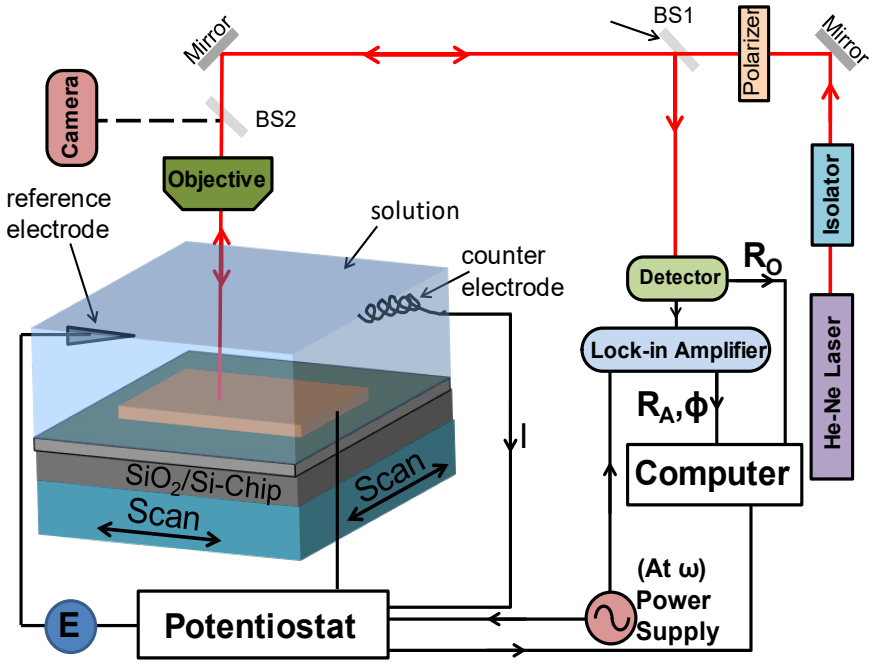

Figure S4. Schematic of SEED set-up.

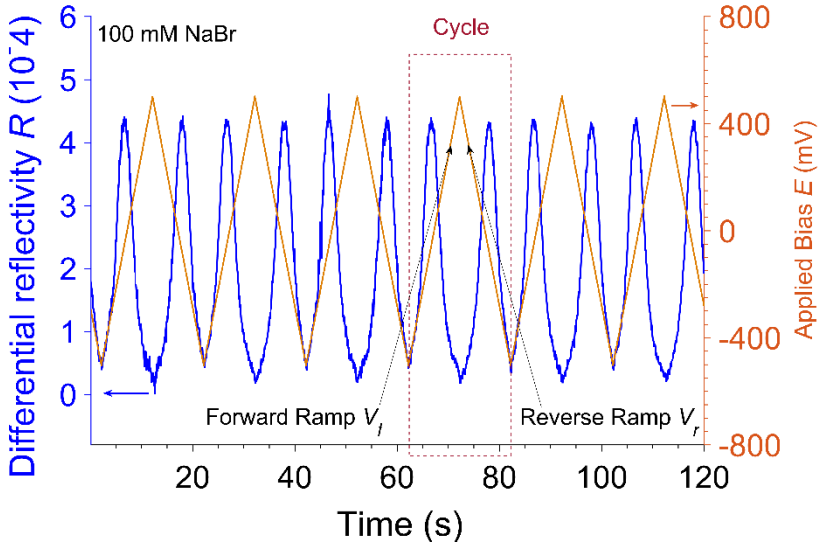

Figure S5. Typical (raw data) output from SEED. The applied bias is the CV ramp and *R* is the differential reflectivity measured by SEED. Forward and reverse ramps are rising and falling CV potentials.

S5. Measurement of deposition rate by SEED

Real time deposition was followed by measuring R at fixed bias (E_{dep}) during 10 min. Raw data of solutions containing PE showed linear decay at various fixed potentials between the working electrode and the solution. Larger decay was observed near PZC of the corresponding salt present in the solution (Figure S6a-c). In solutions containing only salt, R decay was negligible (Figure S6d,e). Errors were calculated as deviation of the linear regression from raw data. Less than 5% error was found for all data point in each set. Error bars are not noticeable as they are inside of the data point (Figure 4 and S7)

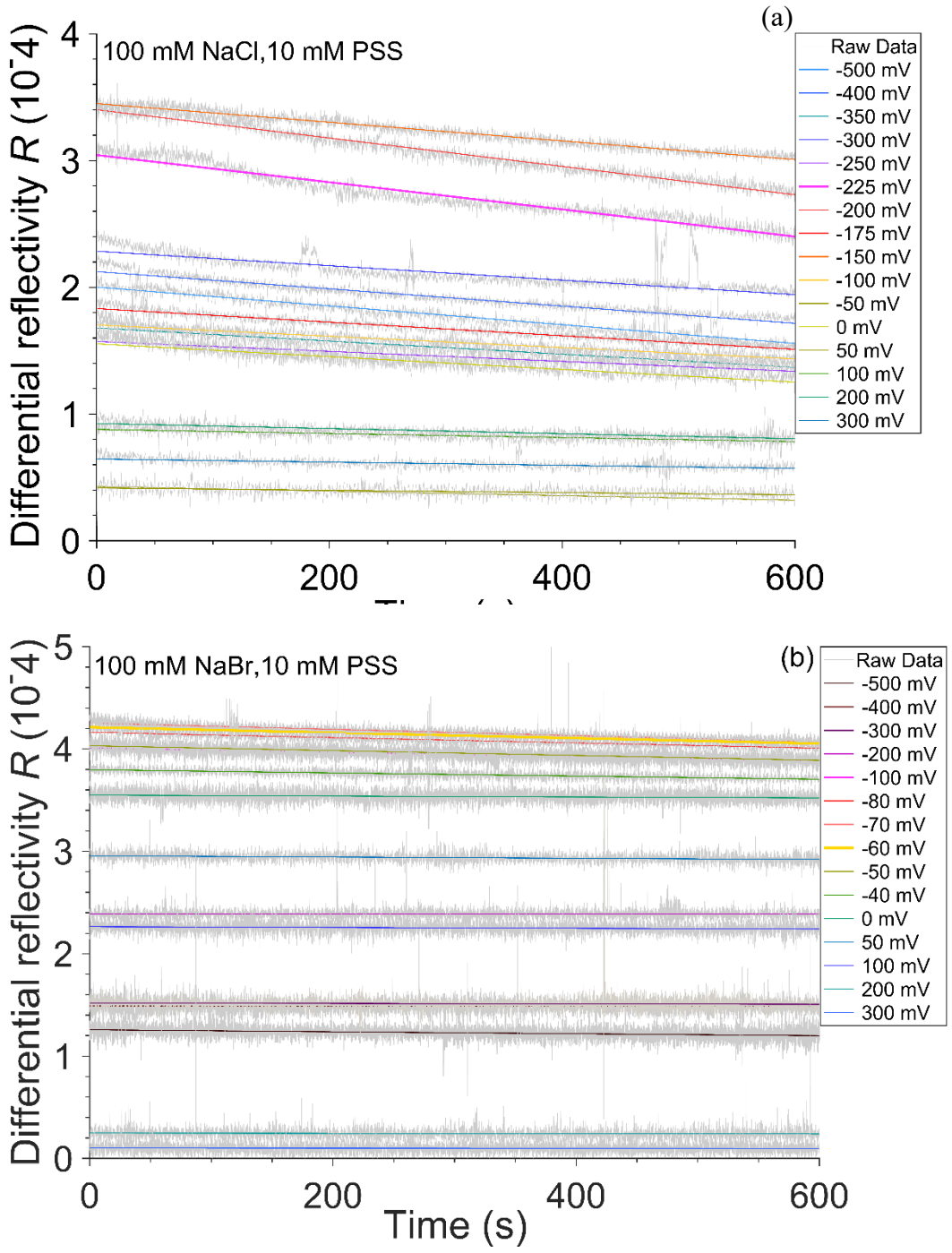

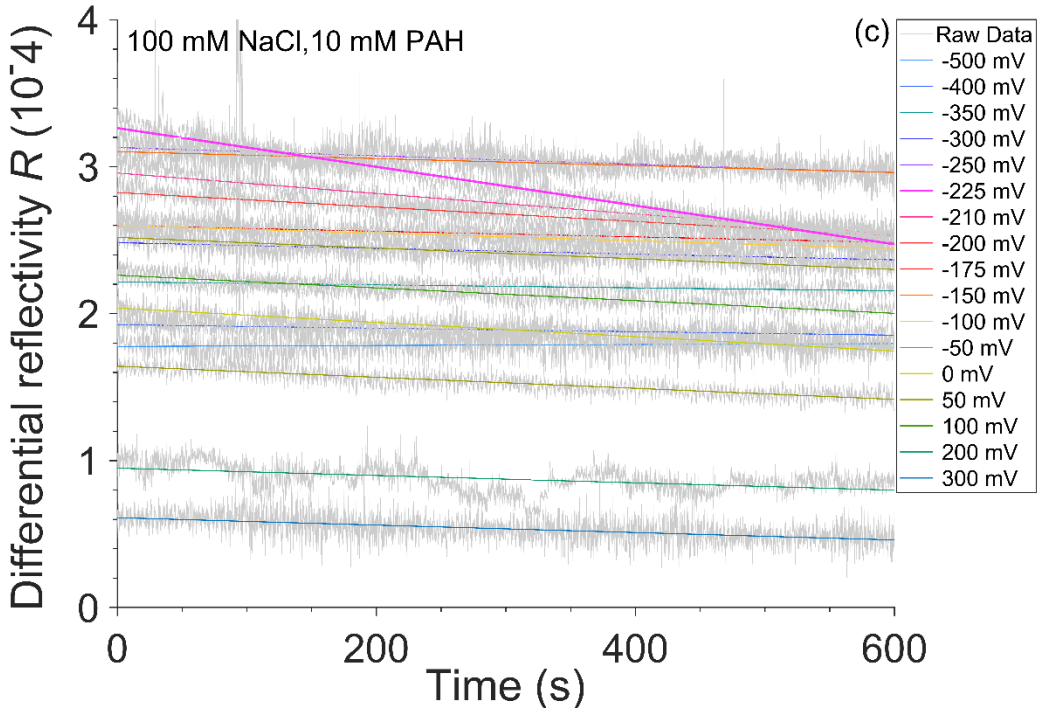
100 mM NaCl,10 mM PAH
(c)
Raw Data
-500 mV
-400 mV
-350 mV
-300 mV
-250 mV
-225 mV
-210 mV
-200 mV
-175 mV
-150 mV
-100 mV
-50 mV
0 mV
50 mV
100 mV
200 mV
300 mV
Differential reflectivity R (10^-4)
Time (s)
0
1
2
3
4
0
200
400
600

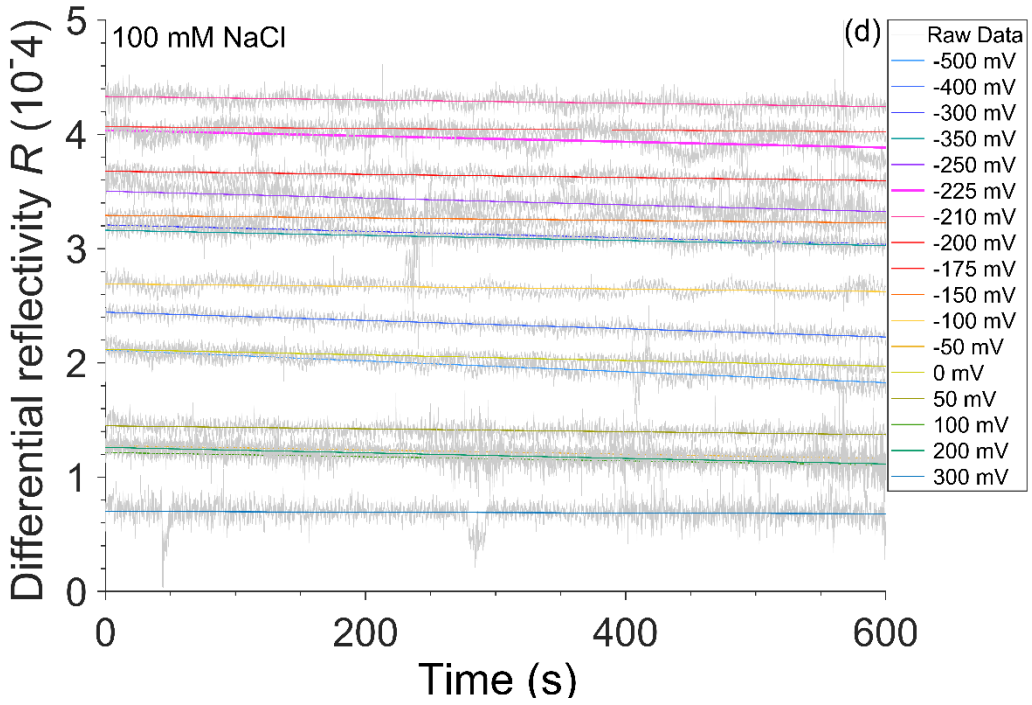
100 mM NaCl
(d)
Raw Data
-500 mV
-400 mV
-300 mV
-350 mV
-250 mV
-225 mV
-210 mV
-200 mV
-175 mV
-150 mV
-100 mV
-50 mV
0 mV
50 mV
100 mV
200 mV
300 mV
Differential reflectivity R (10^-4)
Time (s)
0
1
2
3
4
5
0
200
400
600

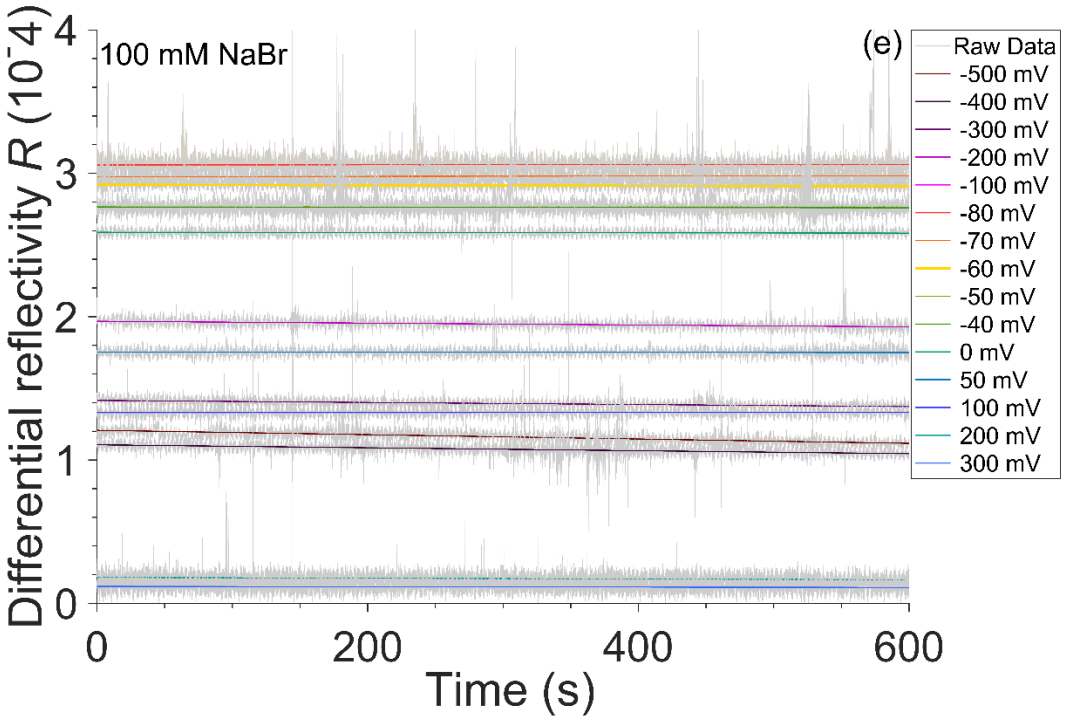

Figure S6. Raw differential reflectivity (*R*) data; Panels (a) to (c) show *R* decay for PE and salt present in the solution. Panels (d) and (e) show *R* decay for only salt present in the solution.

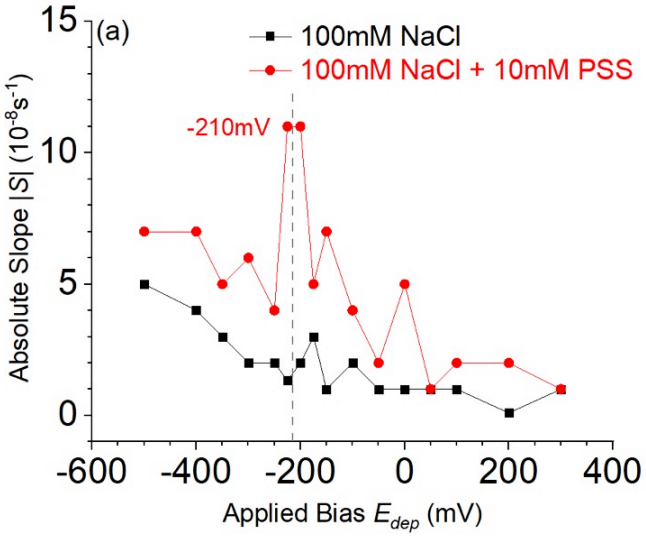

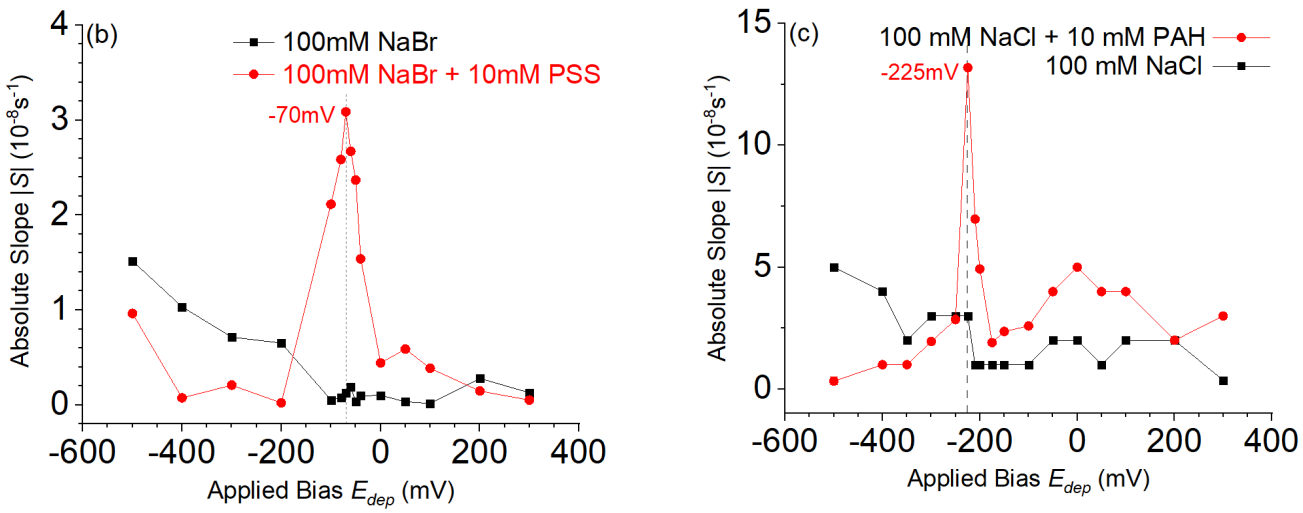

Figure S7. Rate of deposition measured by SEED. The data is reproduced from Fig. 4 with an added curve for control showing no peak in the absence of the PE. The panels (a) to (c) are for different PE and E_{dep} conditions (shown in Fig. 1).

S6. Summary of Peak values

System	V_z (mV)	E_{dep} (mV) at $\lvert V_{z,0} - V_o \rvert_P$ max	$\lvert V_{z,0} - V_o \rvert_P$ max (mV)	E_{dep} (mV) at $\lvert S \rvert$ max	$\lvert S \rvert$ max (10^{-8} s^{-1})
100 mM NaCl	-240.0	N/A	N/A	N/A	N/A
100 mM NaBr	-60.0	N/A	N/A	N/A	N/A
10 mM PSS - 100 mM NaCl	-210.0	-240.0	187.9	-210.0	11.0
10 mM PSS - 100 mM NaBr	-80.0	-60.0	192.6	-70.0	3.1
10 mM PAH - 100 mM NaCl	-250.0	-240.0	167.9	-225.0	13.2
10 mM PAH - 100 mM NaBr	250.0	N/A	N/A	N/A	N/A

S7. Anomalous behavior on NaBr/PAH System

Although the PAH/NaBr system is not further pursued in this study the anomalous behavior is conjectured. The anomalous behavior of NaBr may be attributed to the formation of strong specific bond between Br- and Au in contrast to a much weaker bond with Cl^- [7]. When anions bond specifically on the gold surface, surface reconstruction can occur shifting the PZC. Moreover, at low pH it has been shown that gold PZC can change up to 300 mV due to surface reconstruction. This might explain why the anomalous behavior is only present in PAH solutions (pH 4.6) and not in PSS (pH 8.0).[8] Only V_z data for 10 mM PAH – 100mM NaBr system is reported in Table 1.

References

1. Lee, S. W.; Lopez, J.; Saraf, R. F. Direct mapping of local redox current density on a monolith electrode by laser scanning. *Biosensors & Bioelectronics* **2013,** *47*, 408-414.

2. Lee, S. W.; Lopez, J.; Saraf, R. F. Fabrication and Properties of Redox Ion Doped Few Monolayer Thick Polyelectrolyte Film for Electrochemical Biosensors at High Sensitivity and Specificity. *Electroanalysis* **2013,** *25* (6), 1557-1566.

3. Singh, G.; Saraf, R. F. Direct measurement of ion accumulation at the electrode electrolyte interface under an oscillatory electric field. *Journal of Physical Chemistry B* **2006,** *110* (25), 12581-12587.

4. Singh, G.; Saraf, R. F. Direct measurement of ion accumulation at the electrode electrolyte interface under an oscillatory electric field. *Journal of Physical Chemistry B* **2006,** *110* (25), 12581-12587.

5. Yu, C. C.; Lee, S. W.; Ong, J.; Moore, D.; Saraf, R. F. Single Electron Transistor in Aqueous Media. *Advanced Materials* **2013,** *25* (22), 3079-3084.

6. Tevatia R.; Prasad A.; Saraf, R. F. Electrochemical Characteristics of a DNA Modified Electrode as a Function of Percent Binding. *Analytical Chemistry* **2019**, 91, 10501-10508.

7. Magnussen O. M. Ordered Anion Adlayers on Metal Electrode Surfaces. *Chemical Reviews*. **2002**, 102, 679−725.

8. Kolb D.M.; Schneider J. Surface Reconstruction in Electrochemistry: Au(100)-(5X20), Au(111)-(1x23) and Au(110)-(1X2). *Electrochimica Acta*. **1986**, 31 (8), 929-936.